Focused X-shaped pulses

Michel Zamboni-Rached

Department of Microwaves and Optics, Faculty of Electrical Engineering, Universidade Estadual de Campinas, Campinas, SP, Brazil

Amr M. Shaarawi

The Physics Department, The American University in Cairo, P.O. Box 2511, Cairo 11511, Egypt

Erasmo Recami

Facoltà di Ingegneria, Università statale di Bergamo, Dalmine (BG) 24044, Italy, and Istituto Nazionale di Fisica Nucleare, Sezione di Milano, Milan, Italy

Received September 21, 2003; revised manuscript received February 26, 2004; accepted March 23, 2004

The space–time focusing of a (continuous) succession of localized X-shaped pulses is obtained by suitably integrating over their speed, i.e., over their axicon angle, thus generalizing a previous (discrete) approach. New superluminal wave pulses are first constructed and then tailored so that they become temporally focused at a chosen spatial point, where the wave field can reach very high intensities for a short time. Results of this kind may find applications in many fields, besides electromagnetism and optics, including acoustics, gravitation, and elementary particle physics. © 2004 Optical Society of America

OCIS codes: 320.5540, 070.1060, 070.2580, 320.5550, 050.1970, 060.4080, 140.3300, 170.0170.

1. INTRODUCTION

For many years it has been known that localized (nondiffractive) solutions exist to the wave equation.[1–3] Some localized wave solutions have peaks that travel at the speed of light, and others are endowed with subluminal or superluminal velocities.[4,5] In more recent years, particular attention has been paid to superluminal[6–9] localized waves (for short review papers, see, e.g., Refs. 10 and 11), which can have several applications, such as high-resolution imaging,[12] secure communications, nondiffractive pulse propagation in material media,[13–16] and identification of buried objects.[17]

The most characteristic superluminal localized waves resulted in the so-called X-shaped solutions, also named X waves in brief (see early Refs. 18, and references therein, and 19 as well as Refs. 6–11, and 20), whose structure and behavior are by now well understood and experimentally reproduced.[21–25] Even their propagation along waveguides has been investigated.[26–29] In addition, their finite-energy versions, with arbitrary frequencies and adjustable bandwidths,[9,14,30] have also been constructed. Moreover, several investigations about constructing and generating approximate X-shaped waves from finite apertures[31–37] have been carried on.

In a recent paper by Shaarawi *et al.*,[38] which appeared in this journal, a space–time focusing technique (called temporal focusing) that used superpositions of localized X waves traveling with different velocities was introduced. The various pulses were designed to reach a given spatial point $z = z_f$ at the same time $t = t_f$. In the aforementioned paper,[38] the resulting composite X-shaped wave was synthesized as a discrete sum of individual X waves. In the present paper we generalize that focusing scheme by going on, in particular, to a continuous superposition of individual X waves, i.e., to integrals (instead of discrete sums). We are, moreover, going to show how one can, in general, use any known superluminal solution to obtain from it a large number of analytic expressions for space–time focused waves, endowed with a very strong intensity peak at a desired location. Finally, we shall consider the case of the excitation of such pulses from finite-size apertures. At variance with the source-free case, the range over which the aperture-generated pulses can be focused is limited by the field depth[6,7,38,39] of the individual X-wave components.

2. SPACE–TIME FOCUSING METHODS

A. The Discrete Temporal Focusing Scheme

Let us first summarize the temporal focusing scheme developed in Ref. 38. Since the velocity of the X-shaped waves depends on their apex angle θ (also known as the axicon angle), the space–time focusing was achieved by superimposing a discrete number of X waves, characterized by different θ values. In this paper we will go on to more efficient superpositions for different velocities V, related to θ through the known[6,7,10,11] relation $V = c/\cos\theta$. It will be shown in Section 3 that this enhanced focusing scheme has the advantage of yielding analytic (closed-form) expressions for the spatiotemporally focused pulses.

Consider an axially symmetric superluminal wave pulse $\psi(\rho, z - Vt)$ in a dispersionless medium, where $V > c$ is the pulse velocity and (ρ, ϕ, z) are the cylindrical coordinates. Pulses like these can be obtained by a superposition of Bessel beams,[6,7,11,40] namely,

$$\psi(\rho, z - Vt) = \int_{-\infty}^{\infty} S(\omega) J_0\left(\frac{\omega}{c}\rho \sin\theta\right) \times \exp\left[i\frac{\omega}{c}\cos\theta\left(z - \frac{c}{\cos\theta}t\right)\right] d\omega, \quad (1)$$

where θ is the Bessel beam axicon angle, with $V = c/\cos\theta$, and $S(\omega)$ is the frequency spectrum. The center of such pulses is located at $z = Vt$. Many solutions of this kind, as well as their finite-energy versions, can be found in Refs. 30 and 9. Incidentally, it should be recalled that superluminal waves, depending on (z, t) only through the combination $\zeta = z - Vt$, have infinite energy. The versions with finite energy, written as $\psi(\rho, z - Vt, z + Vt)$, can be found in Ref. 9. Other types of finite-energy superluminal pulse may be found in Ref. 30.

Let us state first that if $\psi(\rho, z - Vt)$ is a solution of the wave equation, then, obviously, $\psi_n(\rho, z - V_n(t - t_n))$, with t_n as a constant, is also a solution. Suppose now that we have N waves of the type $\psi_n(\rho, z - V_n(t - t_n))$, with different velocities, $c < V_1 < V_2 < \ldots < V_N$, and emitted at (different) times t_n, quantities t_n being constants, and $n = 1, 2, \ldots N$. The center of each pulse is located at

$$z = V_n(t - t_n). \quad (2)$$

When we speak of emission or arrival time, we refer to the peak of the traveling pulse; e.g., the emission time is that at which the pulse peak is located at $z = 0$.

To obtain a highly focused wave, we need all wave components $\psi_n(\rho, z - V(t - t_n))$ to reach a given point, $z = z_f$, at the same time $t = t_f$. On choosing $t_1 = 0$ for the slowest pulse ψ_1, it is easily seen that the peak of this pulse reaches the point $z = z_f$ at the time

$$t_f = z_f/V_1. \quad (3)$$

Combining Eqs. (2) and (3), we obtain that for each ψ_n the instant of emission t_n must be

$$t_n = (1/V_1 - 1/V_n)z_f. \quad (4)$$

Therefore a solution of the type

$$\Psi(\rho, z, t) = \sum_{n=1}^{N} A_n \psi_n(\rho, z - V_n(t - t_n)), \quad (5)$$

where A_n are constants, will represent a set of N (initially separated) superluminal waves, which just reach the position $z = z_f$ at the same time $t = t_f = z_f/V_1$.

The scheme described above was essentially developed in Ref. 38 by use of discrete X waves: We have just replaced summations over θ with summations over V. In the remaining part of this paper, we propose a generalization of that idea, which can yield new classes of exact superluminal solutions besides providing enhanced focusing effects.

B. The New (Continuous) Space–Time Focusing Scheme

In this subsection we extend the previous temporal focusing approach[38] by considering a continuous superposition, namely, by integrating over the velocity (instead of performing a discrete sum over the angle θ).

Combining Eqs. (4) and (5) and going on to the integration over V, one gets

$$\Psi(\rho, z, t) = \int_{V_{\min}}^{V_{\max}} dV A(V) \times \psi\left(\rho, z - V\left[t - \left(\frac{1}{V_{\min}} - \frac{1}{V}\right)z_f\right]\right), \quad (6)$$

where V is the velocity of the wave ψ in Eq. (1).

One should note that this representation results in a generalization of the important X transform introduced in Ref. 41, which was actually devoted to pulses tailored as superpositions of standard X waves [whereas any superluminal solution can be used as the kernel of the synthesis given in Eq. (6): Examples of superluminal solutions, other than the standard X waves, are the focused X waves,[30] Bessel X pulses,[42] and orthogonal X waves[43] as well as the many solutions presented in Refs. 11, 39, and 44 and particularly in Ref. 9]. The integration over V in Eq. (6) is quite analogous, of course, to the integration over the axicon angle θ, considered in Ref. 41 and elsewhere, that produces the composite X waves, but we are exploiting such composite X waves for producing focused pulses, a possibility first recognized in Ref. 38. Indeed, the integration over V in Eq. (6) will be shown to be extremely effective in tailoring initial field distributions that produce highly focused pulses at a preassigned position.

In the above integration, V is considered a continuous variable in the interval $[V_{\min}, V_{\max}]$. In Eq. (6), $A(V)$ is the velocity distribution function that specifies the contribution of each wave component (with velocity V) to the integration. The resulting wave $\Psi(\rho, z, t)$ can have a more or less strong amplitude peak at $z = z_f$, at time $t_f = z_f/V_{\min}$, depending on $A(V)$ and on the difference $V_{\max} - V_{\min}$. Let us notice that even the resulting wave field will propagate with a superluminal velocity, depending on $A(V)$ too. In the cases in which $A(V)$ can be actually considered a distribution function, namely, when $A(V) > 0$, $\forall V$, and $\int_{V_{\min}}^{V_{\max}} dV A(V) < \infty$, we can heuristically expect that the mean velocity $\bar{V}$ of the field [Eq. (6)] will be

$$\bar{V} \approx \frac{\int_{V_{\min}}^{V_{\max}} A(V) V dV}{\int_{V_{\min}}^{V_{\max}} A(V) dV} > c. \quad (7)$$

In the cases in which the velocity distribution function is well concentrated around a certain velocity value, one can expect the wave [Eq. (6)] to increase its magnitude and spatial localization while propagating. Finally, the pulse peak acquires its maximum amplitude and localization (at the chosen point $z = z_f$ and at time $t = z_f/V_{\min}$, as we know). Afterward, the wave suffers a progressive spreading and a decrease of its amplitude.

3. ENHANCED FOCUSING EFFECTS BY USE OF ORDINARY X WAVES

Here we present a specific example by integrating, in Eq. (6), over the standard, ordinary[6,7] X waves:

$$X(\rho, z - Vt) = \frac{V}{\left\{[aV - i(z - Vt)]^2 + \left(\frac{V^2}{c^2} - 1\right)\rho^2\right\}^{1/2}}. \tag{8}$$

The classical solution (8) can be obtained[6,9,7] by substituting the spectrum $S(\omega) = \Omega(\omega)\exp(-a\omega)$ into Eq. (1), where a is a constant that defines the bandwidth, $\Delta\omega = 1/a$, and $\Omega(\omega)$ is the step function. (The step function, or Heaviside function, assumes the values $\Omega = 0$ for $\omega < 0$ and $\Omega = 1$ for $\omega \geqslant 0$, as is well known.) When the zeroth-order X waves above are used, however, the largest spectral amplitudes are obtained for low frequencies. For this reason, one may expect that the solutions considered below will be suitable mainly for low-frequency applications.

Let us choose, then, the function ψ in the integrand of Eq. (6) to be $\psi(\rho, z, t) \equiv X\{\rho, z - V[t - (1/V_{\min} - 1/V)z_f]\}$, viz.,

$$\psi(\rho, z, t) \equiv X = \frac{V}{\left[\left(aV - i\left\{z - V\left[t - \left(\frac{1}{V_{\min}} - \frac{1}{V}\right)z_f\right]\right\}\right)^2 + (V^2/c^2 - 1)\rho^2\right]^{1/2}}. \tag{9}$$

After some manipulations, one obtains the analytic integral solution

$$\Psi(\rho, z, t) = \int_{V_{\min}}^{V_{\max}} \frac{VA(V)}{\sqrt{PV^2 + QV + R}}\,dV, \tag{10}$$

with

$$P = \left\{\left[a + i\left(t - \frac{z_f}{V_{\min}}\right)\right]^2 + \frac{\rho^2}{c^2}\right\},$$

$$Q = 2\left(t - \frac{z_f}{V_{\min}} - ai\right)(z - z_f),$$

$$R = [-(z - z_f)^2 - \rho^2]. \tag{11}$$

In what follows, we illustrate the behavior of our new spatiotemporally focused pulses by taking into consideration four different velocity distributions $A(V)$.

In the first case: Let us consider our integral solution (10) with

$$A(V) = 1. \tag{12}$$

In this case, the contribution of the X waves is the same for all velocities in the allowed range $[V_{\min}, V_{\max}]$, and Eq. (10) yields

$$\Psi(\rho, z, t) = \int_{V_{\min}}^{V_{\max}} \frac{V}{\sqrt{PV^2 + QV + R}}\,dV. \tag{13}$$

On using the identity 2.261 in Ref. 45, we obtain the new particular solution

$$\Psi(\rho, z, t) = \frac{\sqrt{PV_{\max}^2 + QV_{\max} + R} - \sqrt{PV_{\min}^2 + QV_{\min} + R}}{P} + \frac{Q}{2P^{3/2}}\ln\left[\frac{2\sqrt{P(PV_{\min}^2 + QV_{\min} + R)} + 2PV_{\min} + Q}{2\sqrt{P(PV_{\max}^2 + QV_{\max} + R)} + 2PV_{\max} + Q}\right], \tag{14}$$

where P, Q, and R are given in Eqs. (11). A three-dimensional (3-D) plot of this function is provided in Fig. 1, where we have chosen $a = 10^{-12}$ s, $V_{\min} = 1.001\ c$, $V_{\max} = 1.005\ c$, and $z_f = 200$ cm. It can be seen that this solution exhibits a rather evident space–time focusing. An initially spread-out pulse (shown for $t = 0$) becomes highly localized at $t = t_f = z_f/V_{\min} = 6.66$ ns, the pulse peak amplitude at z_f being 40.82 times greater than the initial one. In addition, at the focusing time t_f the field is much more localized than at any other time. The velocity of this pulse is approximately $\bar{V} = 1.003\ c$.

In the second case: We choose

$$A(V) = 1/V, \tag{15}$$

and Eq. (10) gives

$$\Psi(\rho, z, t) = \int_{V_{\min}}^{V_{\max}} \frac{1}{\sqrt{PV^2 + QV + R}}\,dV. \tag{16}$$

$$\Psi(\rho, z, t) = \frac{1}{\sqrt{P}}\ln\left(\frac{2\sqrt{P(PV_{\max}^2 + QV_{\max} + R)} + 2PV_{\max} + Q}{2\sqrt{P(PV_{\min}^2 + QV_{\min} + R)} + 2PV_{\min} + Q}\right). \tag{17}$$

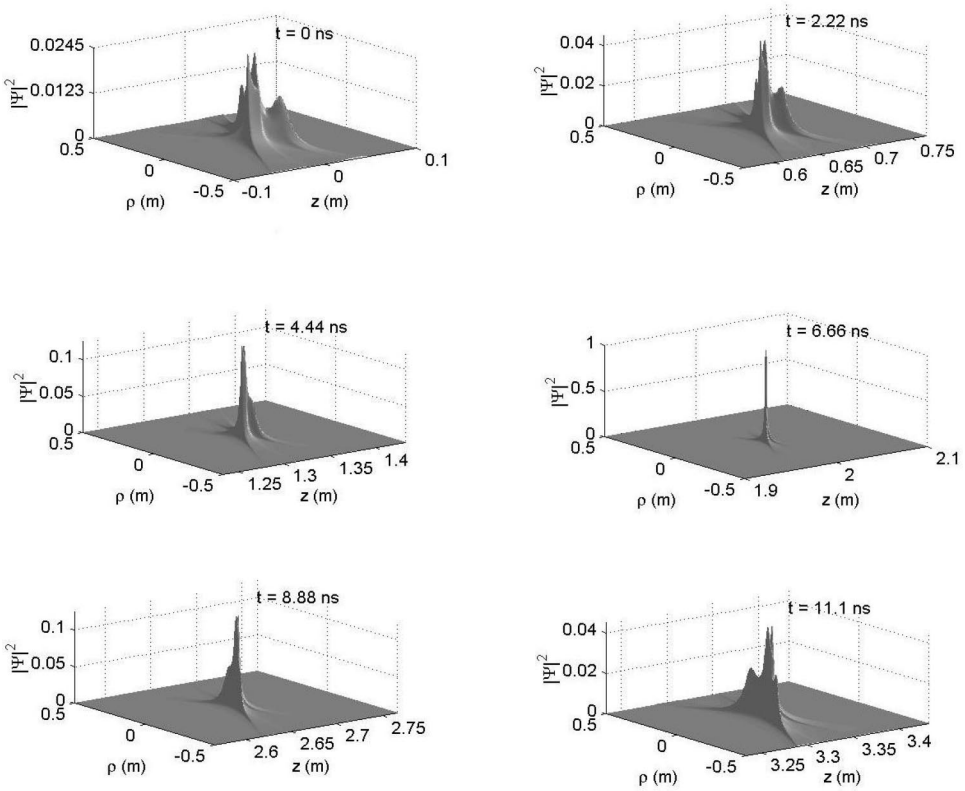

Fig. 1. Space–time evolution of the superluminal pulse represented by Eq. (14); the chosen parameter values are $a = 10^{-12}$ s, $V_{min} = 1.001\ c$, and $V_{max} = 1.005\ c$, and the focusing point is at $z_f = 200$ cm. One can see that this solution is associated with a rather good spatiotemporal focusing: The field amplitude at $z = z_f$ is 40.82 times larger than the initial one. The field amplitude is normalized at the space–time point $\rho = 0, z = z_f, t = t_f$.

In the third case: On substituting the velocity distribution function

$$A(V) = 1/V^2 \tag{18}$$

into Eq. (10), one gets

$$\Psi(\rho, z, t) = \int_{V_{min}}^{V_{max}} \frac{1}{V\sqrt{PV^2 + QV + R}}\,dV. \tag{19}$$

Because of the identity 2.269.1 in Ref. 45, the above integration yields the further particular solution

$$\Psi(\rho, z, t) = \frac{1}{\sqrt{R}} \ln\left\{ \frac{V_{max}[2R + QV_{min} + 2\sqrt{R(PV_{min}^2 + QV_{min} + R)}]}{V_{min}[2R + QV_{max} + 2\sqrt{R(PV_{max}^2 + QV_{max} + R)}]} \right\}. \tag{20}$$

In Fig. 2 the temporal evolution of the superluminal pulse [Eq. (20)] is shown. This solution, too, possesses a good space–time focusing property. This figure has been plotted by use of $a = 10^{-12}$ s, $V_{min} = 1.001\ c$, $V_{max} = 1.005\ c$, and $z_f = 200$ cm. It can be seen that the pulse peak power amplitude at z_f is 40.65 times greater than the initial one. Furthermore, at $t_f = z_f/V_{min}$ the field is much more localized than at any other time. The mean velocity of this pulse is approximately $\bar{V} = V_{min} = 1.0029\ c$.

In the fourth case: With the velocity distribution function given by

$$A(V) = 1/V^3, \tag{21}$$

we have from Eq. (10)

$$\Psi(\rho, z, t) = \int_{V_{min}}^{V_{max}} \frac{1}{V^2\sqrt{PV^2 + QV + R}}\,dV. \tag{22}$$

On using the identity 2.269.2 of Ref. 45, we get the last particular solution

$$\Psi(\rho, z, t) = \frac{\sqrt{PV_{\min}^2 + QV_{\min} + R}}{RV_{\min}} - \frac{\sqrt{PV_{\max}^2 + QV_{\max} + R}}{RV_{\max}}$$

$$+ \frac{Q}{2R^{3/2}} \ln\left\{ \frac{V_{\min}[2\sqrt{R(PV_{\max}^2 + QV_{\max} + R)} + 2R + QV_{\max}]}{V_{\max}[2\sqrt{R(PV_{\min}^2 + QV_{\min} + R)} + 2R + QV_{\min}]} \right\}. \quad (23)$$

4. ENHANCED SPACE–TIME FOCUSING BY USE OF HIGHER-ORDER X WAVES OF ARBITRARY FREQUENCIES AND ADJUSTABLE BANDWIDTHS

The scheme presented in Section 3 (confined to zeroth-order X waves) can be extended to higher-order X waves. Namely, one can use in the integrand of Eq. (6) the various time derivatives of the ordinary X wave, which have been shown[46–48] to constitute an infinite set of generalized X-wave solutions. This procedure will provide us with spatiotemporally focused superluminal pulses that can have any arbitrary frequency and adjustable bandwidth.[9,14] It has also been shown[46–48,11,14,9] that time derivatives of the X waves can be constructed by substituting into Eq. (1) the frequency spectrum $S(\omega) = \Omega(\omega)\omega^m \exp(-a\omega)$, with m an integer. A more general approach for obtaining infinite series of X-shaped solutions through suitable differentiations of the ordinary X wave can be found in Ref. 9, and more details about the properties of the frequency spectra, which allow for closed-form solutions, can be found in the mentioned Refs. 14, 11, and 9.

Namely, by using appropriate values for the parameters m and a, it is possible to shift the central frequency, ω_c, and adjust the bandwidth, $\Delta\omega$, to any desired values.[9,11,14] The relationships among ω_c, $\Delta\omega$, a, and m are

$$\omega_c = m/a,$$

$$m = \frac{1}{\pm\Delta\omega_\pm/\omega_c - \ln(1 \pm \Delta\omega_\pm/\omega_c)}, \quad (24)$$

where[11,14] $\Delta\omega_+ (>0)$ is the bandwidth to the right and $\Delta\omega_- (>0)$ is the bandwidth to the left of ω_c, so that $\Delta\omega = \Delta\omega_+ + \Delta\omega_-$.

It is easy to show that[9,11,14]

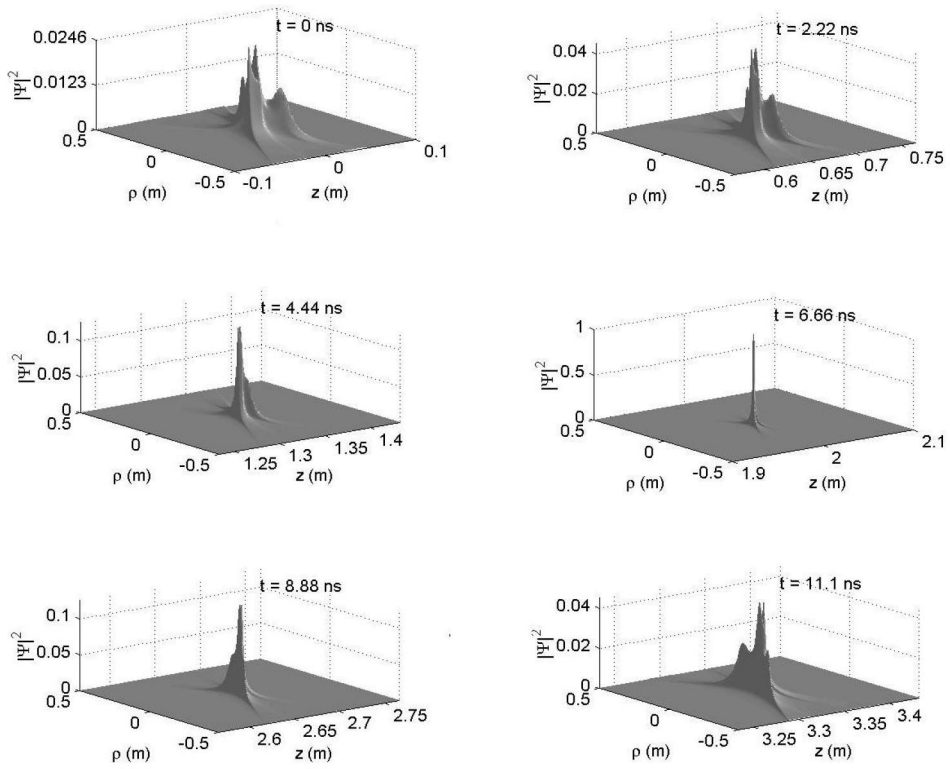

Fig. 2. Space–time evolution of the superluminal pulse represented by Eq. (20), for the same values of the parameters as in Fig. 1 (namely, $a = 10^{-12}$ s, $V_{\min} = 1.001\ c$, and $V_{\max} = 1.005\ c$); the focusing point is again at $z_f = 200$ cm. This solution, too, is associated with a rather good spatiotemporal focusing: The field amplitude at $z = z_f$ is 40.65 times greater than the initial one. The field amplitude is normalized at the space–time point $\rho = 0, z = z_f, t = t_f$.

$$X^{(m)}(\rho, z - Vt) \equiv \int_0^\infty \omega^m \exp(-a\omega) J_0\left(\frac{\omega}{c}\rho \sin\theta\right) \times \exp\left[i\frac{\omega}{c}\cos\theta\left(z - \frac{c}{\cos\theta}t\right)\right] d\omega = i^m \frac{\partial^m X}{\partial t^m}. \quad (25)$$

Let us now choose the function ψ in the integrand of Eq. (6) to be $\psi(\rho, z, t) \equiv i^m X^{(m)}\{\rho, z - V[t - (1/V_{\min} - 1/V)z_f]\}$; Eq. (6) then yields the new (analytic) integral solution

$$\Psi(\rho, z, t) = i^m \frac{\partial^m}{\partial t^m} \int_{V_{\min}}^{V_{\max}} \frac{VA(V)}{\sqrt{PV^2 + QV + R}} dV, \quad (26)$$

with P, Q, and R given by Eqs. (11).

Next, let us consider the cases of four different velocity distributions, similar to the ones used in Subsection 3.A.

As a first example, consider the integration in Eq. (26) with

$$A(V) = 1. \quad (27)$$

On using the result in our previous Eq. (14), we find the particular solution

$$\Psi(\rho, z, t) = i^m \frac{\partial^m}{\partial t^m}\left\{\frac{\sqrt{PV_{\max}^2 + QV_{\max} + R} - \sqrt{PV_{\min}^2 + QV_{\min} + R}}{P} + \frac{Q}{2P^{3/2}} \ln\left[\frac{2\sqrt{P(PV_{\min}^2 + QV_{\min} + R)} + 2PV_{\min} + Q}{2\sqrt{P(PV_{\max}^2 + QV_{\max} + R)} + 2PV_{\max} + Q}\right]\right\}. \quad (28)$$

The plots in Fig. 3 show that this solution implies a great space–time focusing effect. On using $m = 1$, $a = 10^{-12}$ s, $V_{\min} = 1.001\ c$, $V_{\max} = 1.005\ c$, and $z_f = 200$ cm, one finds that the peak amplitude at $z = z_f$ is 1000 times larger than the initial one, and, at the focusing time $t_f = 6.66$ ns, the field is much more localized than at any other time. The velocity of this pulse is approximately $\bar{V} = 1.0029\ c$.

As a second example, let us substitute

$$A(V) = 1/V \quad (29)$$

into Eq. (26). On using the result in Eq. (17), one finds the new particular solution

$$\Psi(\rho, z, t) = i^m \frac{\partial^m}{\partial t^m}\left\{\frac{1}{\sqrt{P}} \times \ln\left[\frac{2\sqrt{P(PV_{\max}^2 + QV_{\max} + R)} + 2PV_{\max} + Q}{2\sqrt{P(PV_{\min}^2 + QV_{\min} + R)} + 2PV_{\min} + Q}\right]\right\}. \quad (30)$$

As a third example, on considering the velocity spectrum

$$A(V) = 1/V^2, \quad (31)$$

we obtain, after combining Eqs. (26) and (20), the further particular solution

$$\Psi(\rho, z, t) = i^m \frac{\partial^m}{\partial t^m}\left(\frac{1}{\sqrt{R}} \ln\left\{\frac{V_{\max}[2R + QV_{\min} + 2\sqrt{R(PV_{\min}^2 + QV_{\min} + R)}]}{V_{\min}[2R + QV_{\max} + 2\sqrt{R(PV_{\max}^2 + QV_{\max} + R)}]}\right\}\right), \quad (32)$$

The plots in Fig. 3 show that this solution implies a great space–time focusing effect. On using $m = 1$, $a = 10^{-12}$ s, $V_{\min} = 1.001\ c$, $V_{\max} = 1.005\ c$, and $z_f = 200$ cm, one finds that the peak amplitude at $z = z_f$ is 1000 times larger than the initial one, and, at the focusing time $t_f = 6.66$ ns, the field is much more localized than at any other time. The velocity of this pulse is approximately $\bar{V} = 1.0029\ c$.

As a fourth example, on substituting the velocity spectrum

$$A(V) = 1/V^3$$

into Eq. (26) and using the result (23), we get the last particular solution

$$\Psi(\rho, z, t) = i^m \frac{\partial^m}{\partial t^m}\left(\frac{\sqrt{PV_{\min}^2 + QV_{\min} + R}}{RV_{\min}} - \frac{\sqrt{PV_{\max}^2 + QV_{\max} + R}}{RV_{\max}} + \frac{Q}{2R^{3/2}} \ln\left\{\frac{V_{\min}[2\sqrt{R(PV_{\max}^2 + QV_{\max} + R)} + 2R + QV_{\max}]}{V_{\max}[2\sqrt{R(PV_{\min}^2 + QV_{\min} + R)} + 2R + QV_{\min}]}\right\}\right). \quad (34)$$

5. A MORE GENERAL FORMULATION

The results presented in the preceding sections demonstrate that in Eq. (6) one can utilize any kind of superlu-

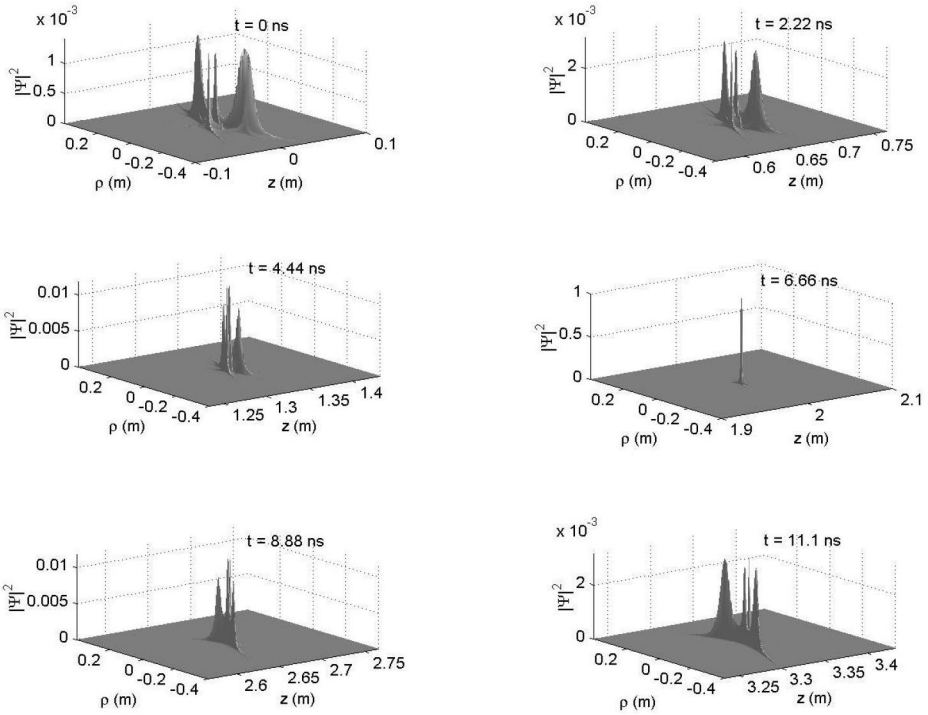

Fig. 3. Space–time evolution of the superluminal pulse represented by Eq. (32). Now the parameters have the values $m = 1$, $a = 10^{-12}$ s (and therefore $\omega_c = 1$ GHz), $V_{\min} = 1.001\ c$, $V_{\max} = 1.005\ c$, and the focusing point is again at $z_f = 200$ cm. This solution, too, is associated with a very good spatiotemporal focusing: The field amplitude at $z = z_f$ is 1000 times higher than the initial one. Once more, the field amplitude is normalized at the space–time point $\rho = 0, z = z_f, t = t_f$.

minal pulse toward the goal of producing large space–time focusing effects. A further generalization of our focusing scheme is introduced in the present section.

Let us recall that a superluminal wave with axial symmetry can be rewritten[9] as a superposition of Bessel beams expressed in terms of V (instead of θ):

$$\psi(\rho, z - Vt) = \int_{-\infty}^{\infty} S(\omega) J_0\left[\frac{\omega}{V}\rho\left(\frac{V^2}{c^2} - 1\right)^{1/2}\right] \times \exp\left[i\frac{\omega}{V}(z - Vt)\right] d\omega, \quad (35)$$

where J_0 is the zeroth-order Bessel function and $S(\omega)$ is the frequency spectrum of the pulse $\psi(\rho, z - Vt)$. Now, by using the focusing method represented by our Eq. (6), one gets

$$\Psi(\rho, z, t) = \int_{V_{\min}}^{V_{\max}} dV A(V) \int_{-\infty}^{\infty} S(\omega) J_0\left[\frac{\omega}{V}\rho\left(\frac{V^2}{c^2} - 1\right)^{1/2}\right] \times \exp\left(i\frac{\omega}{V}\left\{z - V\left[t - \left(\frac{1}{V_{\min}} - \frac{1}{V}\right)z_f\right]\right\}\right) d\omega, \quad (36)$$

which can be rewritten as

$$\Psi(\rho, z, t) = \int_{V_{\min}}^{V_{\max}} dV \int_{-\infty}^{\infty} B(\omega, V) J_0\left[\frac{\omega}{V}\rho\left(\frac{V^2}{c^2} - 1\right)^{1/2}\right] \times \exp\left[i\frac{\omega}{V}(z - Vt)\right] \times \exp\left[i\omega\left(\frac{1}{V_{\min}} - \frac{1}{V}\right)z_f\right] d\omega. \quad (37)$$

Let us briefly mention the question of finite energies. The wave solution $\Psi(\rho, z, t)$ has a finite-energy content when its V spectrum is square integrable, e.g., when the condition $\int_{V_{\min}}^{V_{\max}} dV \int_{-\infty}^{\infty} d\omega (V/\omega)[(V/c)^2 - 1]^{1/2} |B(\omega, V)|^2 < \infty$ is imposed on the spectrum $B(\omega, V)$. It is possible to show that in this case one gets just a finite-energy solution of the type expounded in Ref. 9, with an intensity maximum suitably shifted in space and, correspondingly, in time. Therefore the best approach toward finite total energies, still with a very interesting space–time focusing, would be the one of starting from finite-energy solutions, as the Superluminal Splash Pulses (which are, by the way, the finite-energy version of the classical X wave) or the Superluminal Modified Power Spectrum Solutions of Ref. 9 [Eqs. (17)–(17b) and (18)–(18b) therein, respectively] or the Modified Focused X-Waves of Ref. 30 [Eq. (4.6) therein], and then integrating over V with a square integrable V spectrum. Indeed, in such a way one would be actually superposing localized (finite-energy) waves with different speeds. But such a program, marginal with respect to our present aims, cannot find room in this paper.

From Eq. (37) it can be inferred that frequency-velocity weight functions of the form

$$\bar{S}(\omega, V) \equiv B(\omega, V)\exp\left[i\omega\left(\frac{1}{V_{\min}} - \frac{1}{V}\right)z_f\right] \qquad (38)$$

are able to produce spatiotemporally focused pulses that propagate, once more, at superluminal speeds. Such pulses can be considered a continuous superposition of Bessel beams of different frequencies and different velocities. Moreover, each Bessel beam, endowed with velocity V and angular frequency ω, also possesses a different phase with respect to the others, given by $\exp[i\omega(1/V_{\min} - 1/V)z_f]$. In other words, the frequency-velocity spectra, generators of focused superluminal pulses, determine not only the amplitudes of each Bessel beam in the superposition but also the relative phases among them. Along similar lines, Mugnai *et al.*[49] and Toraldo di Francia[50] demonstrated that one can generate beams with a very high optical resolving power by a superposition of Bessel beams with suitably chosen relative phase delays. This was achieved by the use of a paraffin torus in each one of the coronas adopted for producing the various Bessel beams, the required phase delays being determined by the paraffin. In a sense, the superpositions introduced in this paper appear to reveal that an analogous phenomenon holds in the case of pulses, too.

6. FOCUSED PULSES GENERATED FROM FINITE APERTURES

In the preceding sections we have demonstrated the effectiveness of our space–time focusing scheme in the case of source-free (composite) X-wave pulses. The analysis presented in Section 5 can be actually regarded as a powerful tool that may be used to tailor an initially spread pulse, with the aim of focusing it at a prechosen point in space–time. The situation becomes more involved, however, when such a tailored pulse is generated from an aperture having a finite radius: In fact, X-wave components having different velocities are characterized by different diffraction-free lengths (or field depths). More specifically, $z_d = D/\{2[(V/c)^2 - 1]^{1/2}\}$, where D is the diameter of the circular aperture.

To appreciate the effect of the finite size of the aperture on the space–time focusing scheme, we calculate the field radiated by a finite aperture by using the Rayleigh–Sommerfeld (II) formula, viz.,

$$\Psi_{\mathrm{RS(II)}}(\rho, z, t) = \int_0^{2\pi} \mathrm{d}\phi' \int_0^{D/2} \mathrm{d}\rho' \rho' \times \frac{1}{2\pi R}\left\{[\Psi] + [\partial_{ct'}\Psi]\frac{z - z'}{R}\right\}. \qquad (39)$$

The quantities enclosed by the square brackets in Eq. (39) are evaluated at the retarded time $ct' = ct - R$. The distance $R = [(z - z')^2 + \rho^2 + \rho'^2 - 2\rho\rho'\cos(\phi - \phi')]^{1/2}$ is the separation between source and observation point. Assuming the initial excitation to be that of Eq. (14), we have calculated the radiated field for the parameters $a = 10^{-12}$ s, $V_{\min} = 1.001\ c$, and $V_{\max} = 1.005\ c$. The aperture radius has been chosen to equal 20 cm. For these parameter values, the diffraction-free lengths associated with the chosen values of $V_{\min}$ and $V_{\max}$ are 447.1 and 199.75 cm, respectively. The crucial factor that determines the focusing power of the tailored pulses is the focusing distance z_f. Unlike the source-free case, the focusing distance is influenced by the finite size of the aperture. For the chosen parameters, all X-wave components undergo very little decay over distances $z < 199.75$ cm. In contrast, most of the X-wave components will be decaying at a very fast rate for $z > 447.1$ cm. In the intermediate range $199.75 < z < 447.1$ cm, an increasing portion of the components will decay as the distance from the source increases.

To illustrate the behavior described above, we provide plots of the axial profiles of the generated power $|\Psi|^2$ for $z_f = 200$ and 300 cm. The first focusing point is chosen at the edge of the diffraction-free region, and the second

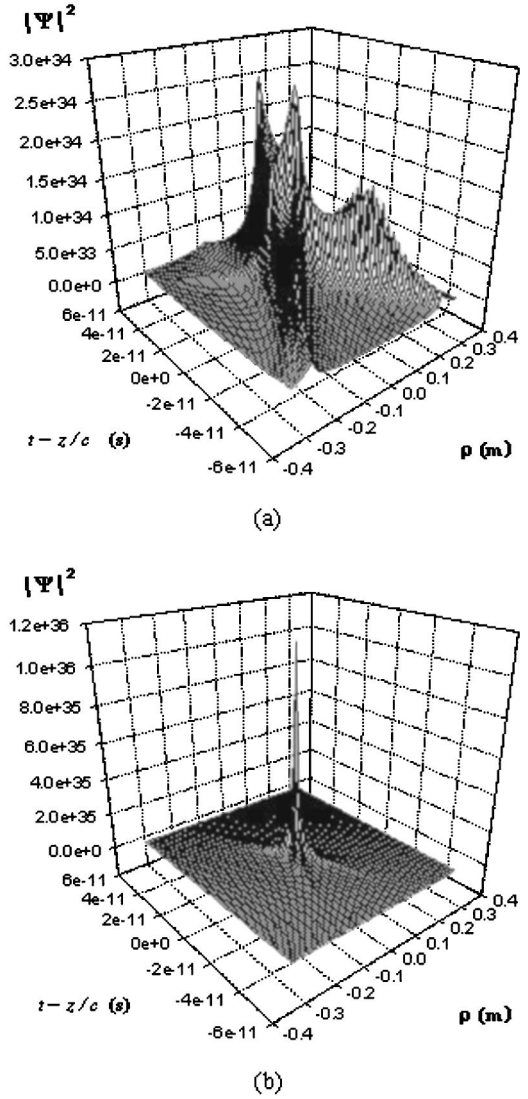

Fig. 4. Surface plots of (a) the initial excitation $|\Psi|^2$ on the aperture plane $z' = 0$ and (b) the source-free pulse at the focusing point $z = z_f = 200$ cm. The spatiotemporally focused pulse corresponds to $a = 10^{-12}$ s, $V_{\min} = 1.001\ c$, and $V_{\max} = 1.005\ c$. The radius of the aperture is chosen equal to 20 cm.

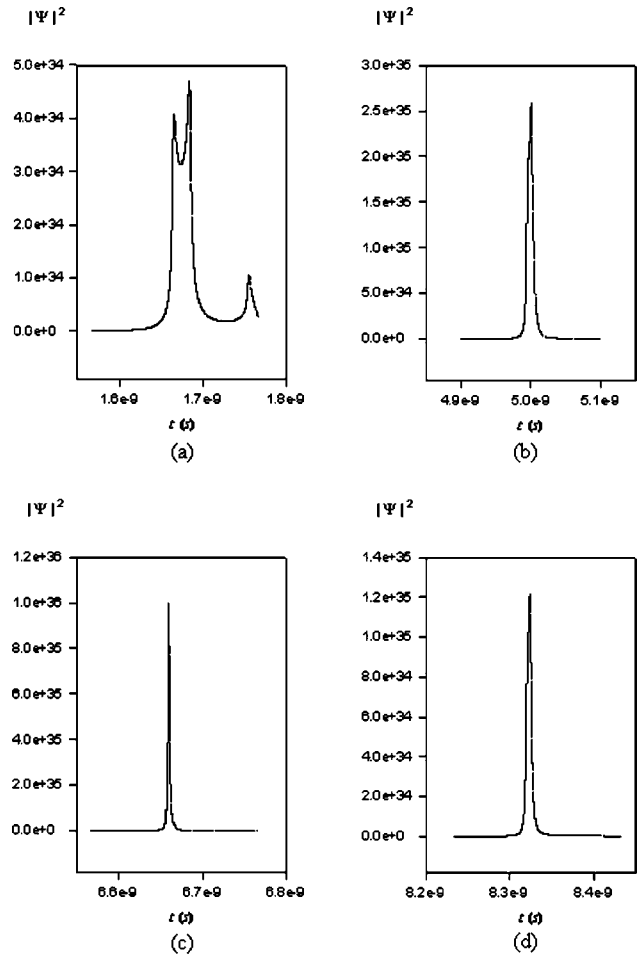

Fig. 5. Axial profiles of the field $|\Psi|^2$ radiated from a finite aperture at distances z = (a) 50, (b) 150, (c) 200, (d) 250 cm. All the other parameters are chosen as in Fig. 4.

is chosen in the middle of the intermediate region. The plots displayed in Figs. 4 and 5 depict the behavior of the pulse radiated from a finite-size aperture for $z_f = 200$ cm. The 3-D surface plots in Fig. 4 show the shape of the initial excitation on the aperture plane $z' = 0$ and the shape of the source-free pulse at the focusing point $z = z_f = 200$ cm. In Fig. 5, we provide plots of the axial profiles of the field radiated from the finite aperture at distances z = 50, 150, 200, and 250 cm. One should notice that the focusing amplitude is comparable with that of the focused source-free pulse at $z = z_f$. The 3-D plot of the focused pulse radiated from the aperture is therefore expected to be similar to the one shown in Fig. 4(b) for the source-free pulse. The plots in Figs. 4 and 5 show, furthermore, that the peak power of the pulse is amplified 40 times. The fact that at $z = 200$ cm the pulse radiated from the aperture resembles the source-free pulse is a confirmation of our qualitative prediction that, for distances $z < 199.75$ cm, all X-wave components contributing to the initial excitation of the source are diffraction free.

As a second example, we have chosen $z_f = 300$ cm. Keeping all the other parameters equal to the ones used for Figs. 4 and 5, we find that the peak power of the aperture-radiated pulse at the focusing point is lower than that of the source-free pulse. The 3-D plots in Fig. 6 show the source-free pulse at the aperture plane and at $z = z_f = 300$ cm. The axial profile of the pulse generated from the finite aperture is shown in Fig. 7 for z = 75, 225, 285, and 375 cm. The peak at $z = z_f = 300$ cm is not shown because the peak focusing occurs, instead, at $z = 285$ cm. This is another manifestation of the fact that contributions from certain X-wave components, constituting the initial excitation, are lost because such components have surpassed their diffraction-free range. Another confirmation of this behavior is that the peak power is amplified ten times only, instead of the 75 times expected for the source-free pulse.

Although the influence of the size of the aperture has been demonstrated only for the pulse given in Eq. (14),

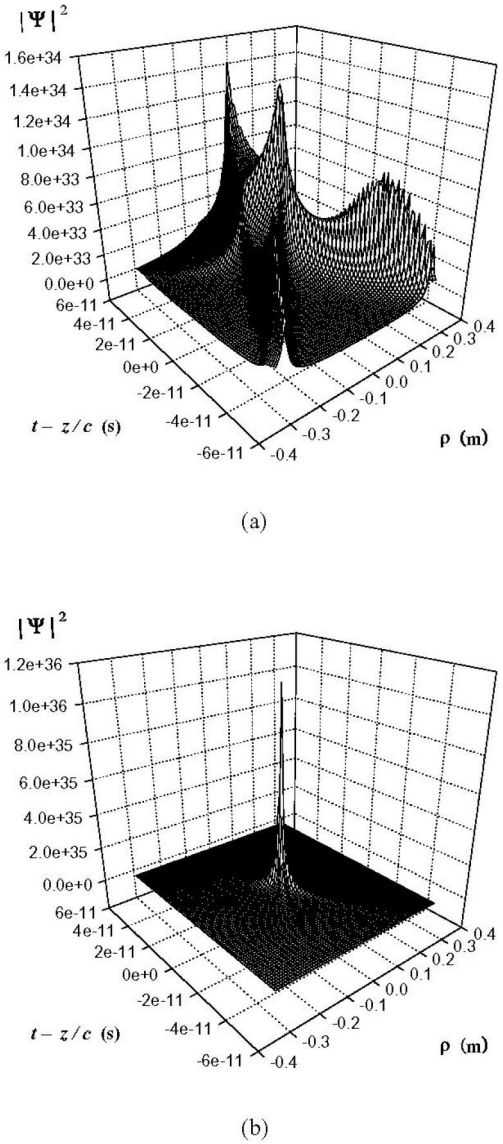

Fig. 6. Surface plots of (a) the initial excitation $|\Psi|^2$ on the aperture plane $z' = 0$ and (b) the source-free pulse at the focusing point $z = z_f = 300$ cm. The spatiotemporally focused pulse has $a = 10^{-12}$ s, $V_{\min} = 1.001\ c$, and $V_{\max} = 1.005\ c$. The radius of the aperture is chosen equal to 20 cm.

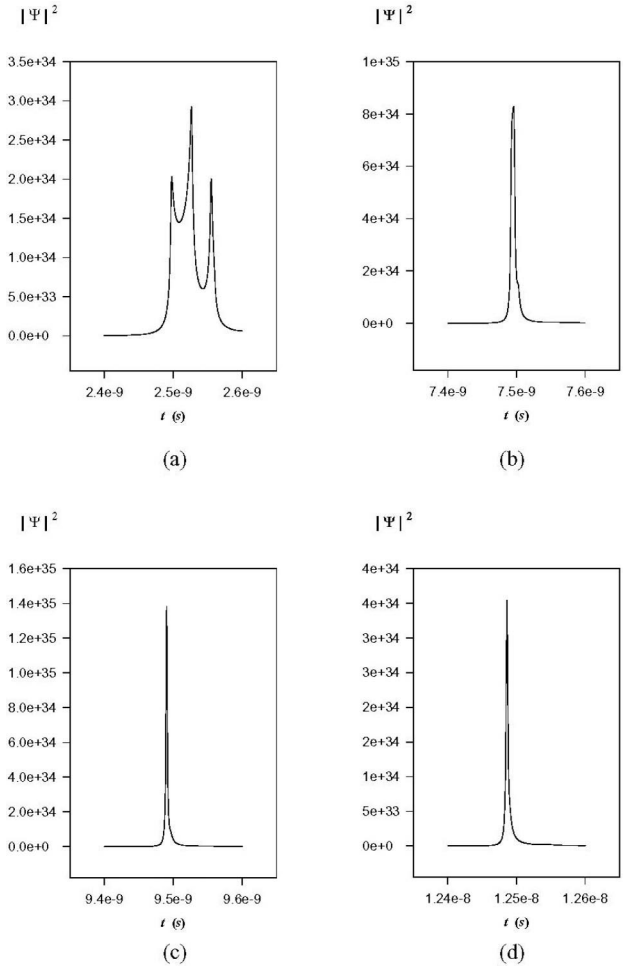

Fig. 7. Axial profiles of the field $|\Psi|^2$ radiated from a finite aperture at distances z = (a) 75, (b) 225, (c) 285, (d) 375 cm. All the other parameters are chosen as in Fig. 6.

one can easily extend the same analysis to spatiotemporally focused pulses of other types [cf. Eqs. (17), (20), and (23)].

7. CONCLUSIONS

In conclusion, by a generalization of the discrete temporal focusing method,[38] we have found new classes of superluminal waves. These new closed-form wave solutions show great potential for space–time focusing. Indeed, we can tailor initially spread-out pulses, so that they are strongly focused at a point chosen *a priori* in space–time. In this paper we have demonstrated that these tailored pulses are easily adjustable by varying the velocity spectra of their superluminal wave components.

We have also investigated the influence of having such pulses launched from a finite-size aperture. It has been shown that, since the individual superluminal wave components, from which the focusing pulse is synthesized, have aperture-dependent diffraction-free lengths, the size of the aperture affects the focusing position and magnitude. The described method is very effective when all superluminal wave components are propagating within their diffraction-free range.

ACKNOWLEDGMENTS

This paper was partially supported by the Fundacão de Amparo à Pesquisa do Estado de São Paulo, Brazil, and by Ministero dell' Università, Ricerca Scientifica e Tecnologia, and Istituto Nazionale di Fisica Nucleare, Italy; previously available as e-print physics/0309098. The authors are very grateful to Hugo E. Hernández-Figueroa and K. Z. Nóbrega (FEEC, Unicamp), I. M. Besieris (Virginia Polytechnic Institute), and Jian-yu Lu (Toledo University, Ohio, USA), for continuous discussions and collaboration. Useful discussions are moreover acknowledged with A. M. Attiya and C. A. Dartora, as well as with V. Abate, T. F. Arecchi, F. Bassani, C. Becchi, R. Collina, C. Conti, G. C. Costa, G. Degli Antoni, G. Kurizki, J. M. Madureira, G. Marchesini, M. Mattiuzzi, D. Mugnai, M. Pernici, V. Petrillo, R. Riva, A. Ranfagni, G. Salesi, M. T. Vasconselos, M. Villa, and S. Zamboni-Rached.

The corresponding author, E. Recami, can be reached by e-mail at recami@mi.infn.it. M. Zamboni-Rached and A. M. Shaarawi can be reached by e-mail at mzamboni@dmo.fee.unicamp.br and shaarawi @aucegypt.edu.

A. M. Shaarawi is on leave from the Department of Engineering Physics and Mathematics, Faculty of Engineering, Cairo University, Giza 12211, Egypt.

REFERENCES AND NOTES

1. H. Bateman, *Electrical and Optical Wave Motion* (Cambridge U. Press, Cambridge, UK, 1915).
2. J. A. Stratton, *Electromagnetic Theory* (McGraw-Hill, New York, 1941), p. 356.
3. R. Courant and D. Hilbert, *Methods of Mathematical Physics* (Wiley, New York, 1966), Vol. 2, p. 760.
4. I. M. Besieris, A. M. Shaarawi, and R. W. Ziolkowski, "A bidirectional traveling plane wave representation of exact solutions of the scalar wave equation," J. Math. Phys. **30**, 1254–1269 (1989).
5. R. Donnelly and R. W. Ziolkowski, "Designing localized waves," Proc. R. Soc. London Ser. A **440**, 541–565 (1993). See also Ref. 30 below.
6. J.-Y. Lu and J. F. Greenleaf, "Nondiffracting X-waves: exact solutions to free-space scalar wave equation and their finite aperture realizations," IEEE Trans. Ultrason. Ferroelectr. Freq. Control **39**, 19–31 (1992).
7. E. Recami, "On localized X-shaped superluminal solutions to Maxwell equations," Phys. A **252**, 586–610 (1998) and references therein.
8. R. W. Ziolkowski, I. M. Besieris, and A. M. Shaarawi, "Aperture realizations of exact solutions to homogeneous-wave equations," J. Opt. Soc. Am. A **10**, 75–87 (1993).
9. M. Zamboni-Rached, E. Recami, and H. E. Hernández-Figueroa, "New localized superluminal solutions to the wave equations with finite total energies and arbitrary frequencies," Eur. Phys. J. D **21**, 217–228 (2002).
10. For short review papers, see, for instance, E. Recami, "Superluminal motions? A bird's-eye view of the experimental situation," Found. Phys. **31**, 1119–1135 (2001). Also see Ref. 11.
11. E. Recami, M. Zamboni-Rached, K. Z. Nóbrega, C. A. Dartora, and H. E. Hernández-Figueroa, "On the localized superluminal solutions to the Maxwell equations," IEEE J. Sel. Top. Quantum Electron. **9**, 59–73 (2003).
12. See, e.g., J.-Y. Lu, H.-H. Zou, and J. F. Greenleaf, "Biomedical ultrasound beam forming," Ultrasound Med. Biol. **20**, 403–428 (1994).

13. P. Saari and H. Sõnajalg, "Pulsed Bessel beams," Laser Phys. **7**, 32–39 (1997).
14. M. Zamboni-Rached, K. Z. Nóbrega, H. E. Hernández-Figueroa, and E. Recami, "Localized superluminal solutions to the wave equation in (vacuum or) dispersive media, for arbitrary frequencies and with adjustable bandwidth," (e-print physics/0209101), Opt. Commun. **226**, 15–23 (2003).
15. C. Conti, S. Trillo, P. Di Trapani, G. Valiulis, A. Piskarskas, O. Jedrkiewicz, and J. Trull, "Nonlinear electromagnetic X-waves," Phys. Rev. Lett. **90**, 170406 (2003).
16. M. A. Porras, S. Trillo, C. Conti, and P. Di Trapani, "Paraxial envelope X-waves," Opt. Lett. **28**, 1090–1092 (2003).
17. A. M. Attiya, "Transverse (TE) electromagnetic X-waves: propagation, scattering, diffraction and generation problems," Ph.D. thesis (Cairo University, Cairo, 2001).
18. See E. Recami, "Classical tachyons and possible applications," Riv. Nuovo Cimento **9**(6), 1–178 (1986) and references therein.
19. A. O. Barut, G. D. Maccarrone, and E. Recami, "On the shape of tachyons," Nuovo Cimento A **71**, 509–533 (1982).
20. J. Fagerholm, A. T. Friberg, J. Huttunen, D. P. Morgan, and M. M. Salomaa, "Angular-spectrum representation of nondiffracting X waves," Phys. Rev. E **54**, 4347–4352 (1996).
21. J.-Y. Lu and J. F. Greenleaf, "Experimental verification of nondiffracting X-waves," IEEE Trans. Ultrason. Ferroelectr. Freq. Control **39**, 441–446 (1992). See also Ref. 22.
22. In the case of Ref. 21, the beam speed is larger than the sound (not of the light) speed in the considered medium.
23. P. Saari and K. Reivelt, "Evidence of X-shaped propagation-invariant localized light waves," Phys. Rev. Lett. **79**, 4135–4138 (1997).
24. D. Mugnai, A. Ranfagni, and R. Ruggeri, "Observation of superluminal behaviors in wave propagation," Phys. Rev. Lett. **84**, 4830–4833 (2000).
25. P. Di Trapani, G. Valiulis, A. Piskarskas, O. Jedrkiewicz, J. Trull, C. Conti, and S. Trillo, "Spontaneous formation of nonspreading X-shaped wavepackets" (e-print physics/0303083) in LANL Archives.
26. M. Zamboni-Rached, E. Recami, and F. Fontana, "Superluminal localized solutions to Maxwell equations propagating along a normal-sized waveguide," Phys. Rev. E **64**, 066603 (2001).
27. M. Zamboni-Rached, F. Fontana, and E. Recami, "Superluminal localized solutions to Maxwell equations propagating along a waveguide: the finite-energy case," Phys. Rev. E **67**, 036620 (2003).
28. M. Zamboni-Rached, K. Z. Nóbrega, E. Recami, and H. E. Hernández-Figueroa, "Superluminal X-shaped beams propagating without distortion along a coaxial guide," Phys. Rev. E **66**, 046617 (2002).
29. M. Zamboni-Rached and H. E. Hernández-Figueroa, "A rigorous analysis of localized wave propagation in optical fibers," Opt. Commun. **191**, 49–54 (2000).
30. I. M. Besieris, M. Abdel-Rahman, A. Shaarawi, and A. Chatzipetros, "Two fundamental representations of localized pulse solutions of the scalar wave equation," Prog. Electromagn. Res. **19**, 1–48 (1998).
31. S. He and J. Y. Lu, "Sidelobe reduction of limited-diffraction beams with Chebyshev aperture apodization," J. Acoust. Soc. Am. **107**, 3556–3559 (2000).
32. J.-Y. Lu and S. He, "High frame rate imaging with a small number of array elements," IEEE Trans. Ultrason. Ferroelectr. Freq. Control **46**, 1416–1421 (1999).
33. J.-Y. Lu, "Experimental study of high frame rate imaging with limited-diffraction beams," IEEE Trans. Ultrason. Ferroelectr. Freq. Control **45**, 84–97 (1998).
34. J.-Y. Lu, "Producing bowtie limited-diffraction beams with synthetic array experiments," IEEE Trans. Ultrason. Ferroelectr. Freq. Control **43**, 893–900 (1996).
35. J.-Y. Lu and J. F. Greenleaf, "Producing deep depth of field and depth-independent resolution in NDE with limited-diffraction beams," Ultrason. Imaging **15**, 134–149 (1993).
36. A. A. Chatzipetros, A. M. Shaarawi, I. M. Besieris, and M. Abdel-Rahman, "Aperture synthesis of time-limited X-waves and analysis of their propagation characteristics," J. Acoust. Soc. Am. **103**, 2287–2295 (1998).
37. M. Abdel-Rahman, I. M. Besieris, and A. M. Shaarawi, "A comparative study on the reconstruction of localized pulses," in *Proceedings of the IEEE Southeast Conference* (Institute of Electrical and Electronics Engineers, New York, 1997), pp. 113–117.
38. A. M. Shaarawi, I. M. Besieris, and T. M. Said, "Temporal focusing by use of composite X-waves," J. Opt. Soc. Am. A **20**, 1658–1665 (2003).
39. See, e.g., C. A. Dartora, M. Zamboni-Rached, K. Z. Nóbrega, E. Recami, and H. E. Hernández-Figueroa, "A general formulation for the analysis of scalar limited-diffraction beams using angular modulation: Mathieu and Bessel beams," Opt. Commun. **222**, 75–80 (2003).
40. H. Sõnajalg, M. Rätsep, and P. Saari, "Demonstration of the Bessel-X pulse propagating with strong lateral and longitudinal localization in a dispersive medium," Opt. Lett. **22**, 310–312 (1997).
41. J.-Y. Lu, "An X-wave transform," IEEE Trans. Ultrason. Ferroelectr. Freq. Control **47**, 1472–1481 (2000).
42. P. Saari and H. Sõnajalg, "Pulsed Bessel beams," Laser Phys. **7**, 32–39 (1997).
43. J. Salo, A. T. Friberg, and M. Salomaa, "Orthogonal X-waves," J. Phys. A. **34**, 9319–9327 (2001).
44. M. Zamboni-Rached, K. Z. Nóbrega, H. E. Hernandez, and E. Recami, "Localized superluminal solutions to the wave equation in (vacuum or) dispersive media, for arbitrary frequencies and with adjustable bandwidth," Opt. Commun. **226**, 15–23 (2003).
45. I. S. Gradshteyn and I. M. Ryzhik, *Integrals, Series and Products*, 4th ed. (Academic, New York, 1965).
46. A. T. Friberg, J. Fagerholm, and M. M. Salomaa, "Space-frequency analysis of non-diffracting pulses," Opt. Commun. **136**, 207–212 (1997).
47. J. Fagerholm, A. T. Friberg, J. Huttunen, D. P. Morgan, and M. M. Salomaa, "Angular-spectrum representation of nondiffracting X waves," Phys. Rev. E **54**, 4347–4352 (1996).
48. P. Saari, "Superluminal localized waves of electromagnetic field in vacuo," in *Time's Arrows, Quantum Measurements and Superluminal Behavior*, D. Mugnai, A. Ranfagni, and L. S. Shulman, eds. (C.N.R., Rome, 2001), pp. 37–48.
49. D. Mugnai, A. Ranfagni, and R. Ruggeri, "Pupils with super-resolution," Phys. Lett. A **311**, 77–81 (2003).
50. G. Toraldo di Francia, "Super-gain antennas and optical resolving power," Nuovo Cimento Suppl. **9**, 426–435 (1952).